IN-SITU STUDY OF ATMOSPHERIC ICE

Victor. F. Petrenko* and Michiya Higa
Thayer School of Engineering, Dartmouth College
8000 Cummings Hall, Hanover, NH 03755, USA

ABSTRACT

We present a new approach for calculating liquid water content in growing atmospheric ice (LWCi) from in-situ measurements of both capacitance and conductance. Computer simulations and experimental data analysis of the four different connections between liquid and solid parts of atmospheric ice show that a combination of series and parallel connections is the most appropriate model for calculating LWCi. Assuming this combination model, and using in-situ measurements of both capacitance and conductance, we were able to accurately determine the time-variation of LWCi.

1. INTRODUCTION

The physical properties of atmospheric ice play a crucial role in the icing of structures such as aircraft, helicopters, power lines, and towers (Minsk, 1983). Since the presence of unfrozen water significantly affects these physical properties, the liquid water content in growing atmospheric ice (LWCi) is one of the most important parameters to measure. While intensive theoretical and experimental studies of atmospheric ice have been done (e.g., Bragg *et al.* 1997, Druez *et al.* 1986, Lozowski *et al.* 2001), most were conducted after ice formation was complete and therefore do not provide data about physical properties during the dynamic phase change period. Thus, an in-situ study of LWCi is necessary to fully understand the physical properties of atmospheric ice.

Our approach for measuring LWCi makes use of the well-known fact that ice and water differ greatly in their electrical properties such as their dielectric constant and their electric conductivity (Petrenko and Whitworth 1999). Thus, it's possible to distinguish between water and ice by measuring these electrical properties. This paper describes our approach in detail for using in-situ measurements of both capacitance and conductance to calculate LWCi.

2. EXPERIMENTS

An icing wind tunnel was used to simulate atmospheric icing (Fig. 1). Ice was grown with a fine water-spray under turbulent-flow conditions in a 20 cm x 20 cm test section of the wind tunnel. Water droplets of distilled water were produced by a spray nozzle, manufactured by Spray Systems Co. having air cap #J73160 and fluid cap # J2050, at an air pressure of 140 kPa and a water pressure of 200-350 kPa.

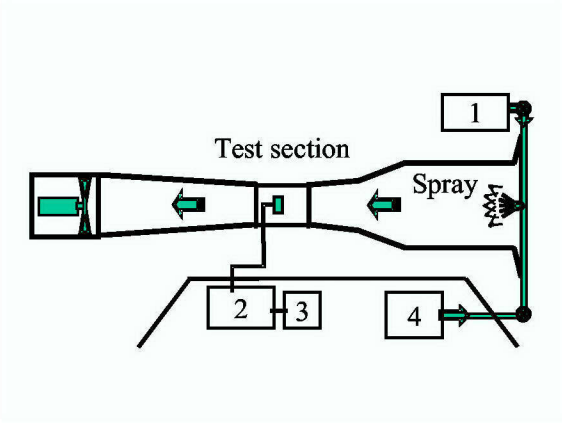

Figure 1. Schematics of experimental setup. 1: Di-water tank (300 ml), 2: HP4192A, 3: PC, 4: Air compressor.

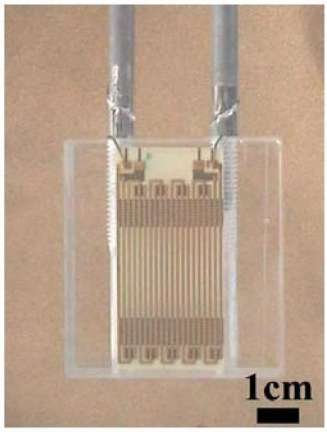

Figure 2. The copper-foil grid electrodes on the ice collector (Plexiglas). The electrodes had a width of 0.68 mm and were spaced at 0.59 mm. The electrode thickness was 0.075 mm.

Report Documentation Page

Form Approved
OMB No. 0704-0188

1. REPORT DATE	2. REPORT TYPE	3. DATES COVERED
00 DEC 2004	**N/A**	**-**

4. TITLE AND SUBTITLE	5a. CONTRACT NUMBER
In-Situ Study Of Atmospheric Ice	5b. GRANT NUMBER
	5c. PROGRAM ELEMENT NUMBER
6. AUTHOR(S)	5d. PROJECT NUMBER
	5e. TASK NUMBER
	5f. WORK UNIT NUMBER
7. PERFORMING ORGANIZATION NAME(S) AND ADDRESS(ES) **Thayer School of Engineering, Dartmouth College 8000 Cummings Hall, Hanover, NH 03755, USA**	8. PERFORMING ORGANIZATION REPORT NUMBER
9. SPONSORING/MONITORING AGENCY NAME(S) AND ADDRESS(ES)	10. SPONSOR/MONITOR'S ACRONYM(S)
	11. SPONSOR/MONITOR'S REPORT NUMBER(S)

12. DISTRIBUTION/AVAILABILITY STATEMENT
Approved for public release, distribution unlimited

13. SUPPLEMENTARY NOTES
See also ADM001736, Proceedings for the Army Science Conference (24th) Held on 29 November - 2 December 2005 in Orlando, Florida. , The original document contains color images.

14. ABSTRACT

15. SUBJECT TERMS

16. SECURITY CLASSIFICATION OF:			17. LIMITATION OF ABSTRACT	18. NUMBER OF PAGES	19a. NAME OF RESPONSIBLE PERSON
a. REPORT **unclassified**	b. ABSTRACT **unclassified**	c. THIS PAGE **unclassified**	**UU**	**6**	

To accurately determine LWCi, we recorded the electrical capacitance at 200 kHz and the electrical conductance at 100 Hz of the atmospheric ice between probe electrodes (Fig. 2) as a function of time both during and after ice growth, using a low-frequency impedance analyzer (HP4192A). The maximum sampling rate in our system was 0.5 Hz. We used copper-foil grid electrodes with a width and thickness of 0.68 mm and 0.075 mm respectively, spaced by 0.59 mm. The measurements were performed at temperatures ranging from –5 to -30 °C, air velocities ranging from 15 to 115 km/h (or from 4.2 to 32 m/s), and varying level of water content in air ranging from 0.1 to 10 g/m3.

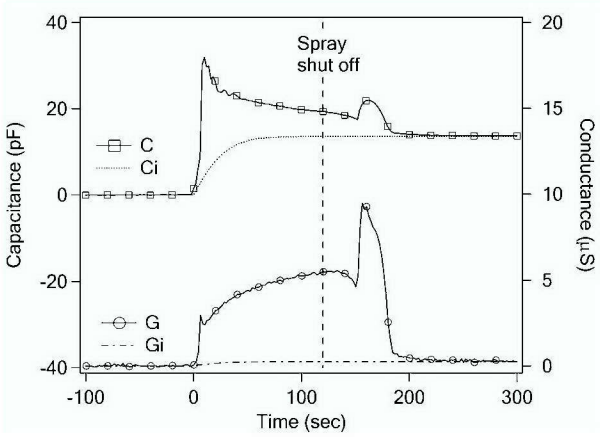

(a)

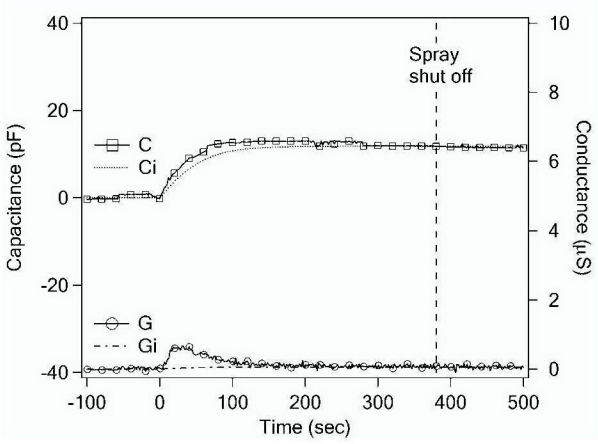

(b)

Figure 3. Typical examples of ice-sample capacitance, C, and conductance, G, vs. time curves. The computed relation between C_i and L_s and that between G_i and L_s as calculated for solid ice are also shown for comparison. (a) Temperature = –10 °C, air speed = 115 km/h, water content in air = 1.67 g/m^3, and ice growth rate = 13.25x10^{-3} mm/sec. (b) Temperature = –30 °C, air speed = 115 km/h, water content in air = 0.25 g/m^3, and ice growth rate = 6.39x10^{-3} mm/sec.

3. RESULTS AND DISCUSSIONS

From our findings, figure 3 shows the typical time-variations of capacitance and conductance of the ice sample. These results not only show that the electrical properties of the simulated atmospheric ice changed significantly when the water spray was turned on and off, but also show a complex time dependence related to the experimental conditions. At a high rate of water flow (high air velocity times water content in air, Fig. 3a) and high temperature, the sample's capacitance, C, monotonically decreased from a value typical for water to one more characteristic of solid ice; while at the same time, the sample's conductance, G, monotonically increased (following a sharp rise upon turning on the water spray). In contrast, at a low rate of water flow and low temperature (Fig. 3b), the capacitance, C, gradually increased at a rate closely corresponding to the increasing solid ice thickness. During ice growth, however, the sample conductance, G, quickly decreased to a level characteristic of solid ice.

Peaks seen on C- and G-curves in Fig. 3a were typical for tests with high rate of water flow after the water spray was shut down. One possible explanation of those peaks is that unfrozen water re-enters ice/grid electrodes interface when liquid inclusions in ice ultimately freeze, perhaps, due to ice fracture.

Since the measured time-variation of the ice sample's capacitance and conductance reflect not only LWCi but also the sample thickness (L_s), we separate these effects using the relationship between C and L_s and that between G and L_s for solid ice. We determined these relationships using the electrostatic model and the conductive media DC model from a FEMLAB software package (Comsol Inc.). This software can solve the electrostatic boundary problem and the steady electric current problem by a finite element method. Figure 4 shows a schematic view of our model's geometry. We performed a simulation of C and G for one unit cell and calculated the total capacitance and conductance of ice sample on the whole surface of the grid electrodes. Insulating boundary conditions are applied to all boundaries except the surface of the electrodes. The dielectric constant and the electric conductivity of ice are set as the values measured in our experiments for each test. Figure 5 shows an example of such simulation for the electric field in the ice using the electrostatic model.

Figure 6 shows the C-L_s curve and the G-L_s curve obtained by the simulation. As seen in Fig. 5, the electric field penetrates in the ice only over a distance comparable with the inter-electrode space ($\approx$0.6mm). Because of this, C and G do not change much after ice thickness exceeds that value, see Fig. 6.

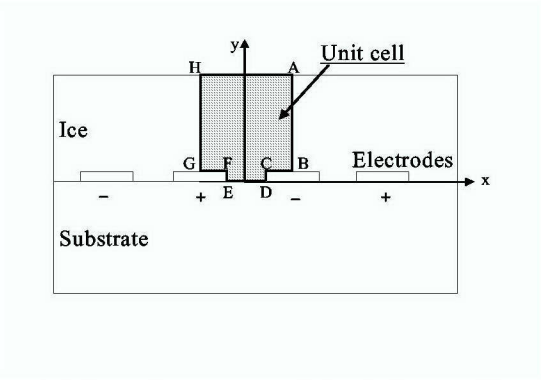

Figure 4. Schematic geometry of simulation model.

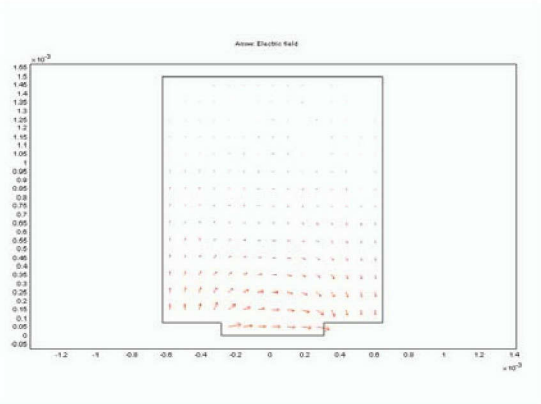

Figure 5. An example of simulation of the electric field in the ice. Ice thickness was 1.5 mm. Arrows show the electric field in the ice. The dielectric constant was set at 2.7.

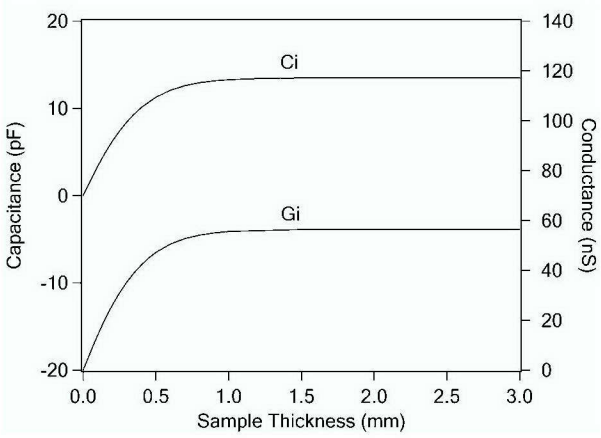

Figure 6. Relationship between the capacitance and the sample thickness and that between the conductance and the sample thickness obtained by a computer simulation for solid ice. The dielectric constant for ice was set at 2.7. The electric conductivity of ice was set at $1x10^{-7}$ S/m.

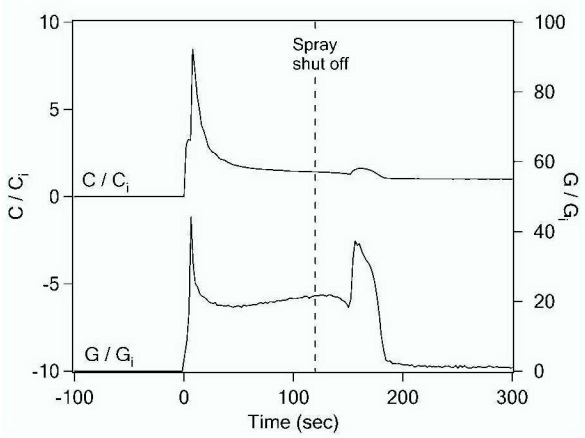

(a)

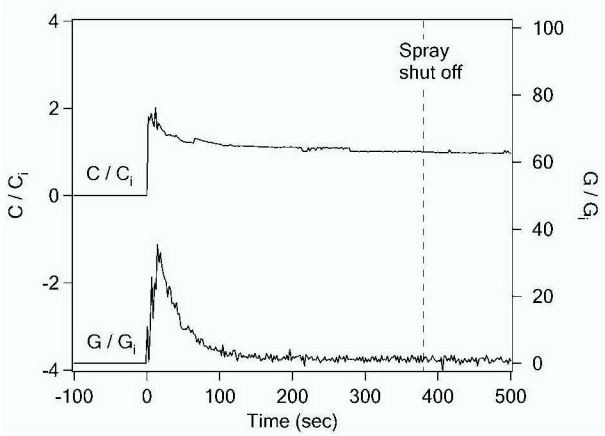

(b)

Figure 7. An example of the time-variations of C/C_i and G/G_i in growing atmospheric ice. (a) Temperature = –10°C, air speed = 115 km/h, water content in air = 1.67 g/m^3, and ice growth rate = $13.25x10^{-3}$ mm/sec. (b) Temperature = –30 °C, air speed = 115 km/h, water content in air = 0.25 g/m^3, and ice growth rate = $6.39x10^{-3}$ mm/sec.

In Figs. 3a&b, the sample thickness effect on ice's capacitance and conductance obtained by the simulation are plotted with the raw data for comparison, where the simulation results are plotted as a function of time assuming the ice growth rate is constant. The data normalized to the sample thickness effect can be expressed in terms of the ratio of C/C_i and G/G_i, where C and G are the sample's capacitance and conductance respectively and C_i and G_i are the sample's capacitance and conductance for liquid-water-free ice respectively (obtained by a simulation). In this way, the data indicate that LWCi approaches zero as these ratios approach one. Figure 7 shows the ratios of C/C_i and G/G_i as a function of time. It's important to remember that what is seen in Fig. 7 is essentially C and G of 0.6-mm thick pre-electrode layer of ice.

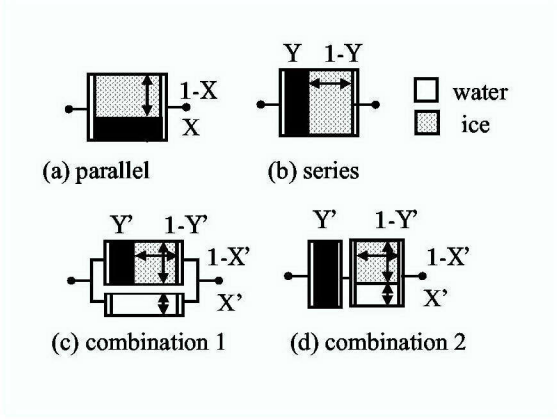

Figure 8. Connection models between water and ice parts in the atmospheric ice.

To determine LWCi using results on ice capacitance and ice conductance, we have to assume some specific type of connections between frozen and unfrozen parts of the ice sample. Figure 8 shows four possible types of such connections:

(a) parallel connection
(b) series connection
(c) combination #1 of parallel and series connections
(d) combination #2 of parallel and series connections

The total capacitance of the sample (C_{total}) for each connection model can be expressed as:

(a) Parallel connection model

$$C_{total} = XC_w + (1-X)C_i, \tag{1}$$

(b) Series connection model

$$C_{total} = \left(\frac{1}{C_w / Y} + \frac{1}{C_i /(1-Y)} \right)^{-1}, \tag{2}$$

(c) Combination model #1

$$C_{total} = X'C_w + (1-X')\left(\frac{1}{C_w / Y'} + \frac{1}{C_i /(1-Y')} \right)^{-1}, \tag{3}$$

(d) Combination model #2

$$C_{total} = \left(\frac{1}{C_w / Y'} + \frac{1}{(X'C_w + (1-X')C_i)/(1-Y')} \right)^{-1}, \tag{4}$$

where X, Y, X' and Y' are fractions of water parts as shown in Fig. 8 and C_w and C_i are the capacitance of the sample when it consists of all water and all ice, respectively. The total capacitance of the sample (G_{total}) for each connection model can be expressed in the same way as C_{total} by replacing C_w and C_i with G_w and G_i, respectively.

If we use the following notations:

$$\begin{aligned} R_c &= C_w / C_i \\ Rg &= G_w / G_i \end{aligned}, \tag{5}$$

LWCi can be solved in terms of C_{total}/C_i, G_{total}/G_i, R_c, and R_g for each connection model as:

(a) Parallel connection model

$$LWCi = X = \frac{\left(\frac{C_{total}}{C_i} - 1 \right)}{(R_c - 1)}, \tag{6}$$

$$LWCi = X = \frac{\left(\frac{G_{total}}{G_i} - 1 \right)}{(R_g - 1)}., \tag{7}$$

(b) Series connection model

$$LWCi = Y = \frac{\left(\frac{C_{total}}{C_i} - 1 \right) R_c}{\frac{C_{total}}{C_i}(R_c - 1)}, \tag{8}$$

$$LWCi = Y = \frac{\left(\frac{G_{total}}{C_i} - 1 \right) R_g}{\frac{G_{total}}{G_i}(R_g - 1)}. \tag{9}$$

(c) Combination model #1

$$LWCi = X' + (1-X')Y', \tag{10}$$

X' and Y' can be solved by the following equations with given C_{total}/C_i, G_{total}/G_i, R_c, and R_g.

$$\frac{C_{total}}{C_i} = \frac{R_c(1 + (R_c - 1)X' - (R_c - 1)X'Y')}{R_c - (R_c - 1)Y'}, \tag{11}$$

$$\frac{G_{total}}{G_i} = \frac{R_g(1 + (R_g - 1)X' - (R_g - 1)X'Y')}{R_g - (R_g - 1)Y'}.$$

(12)

(d) Combination model #2

$$LWCi = (1 - Y')X' + Y', \quad (13)$$

X' and Y' can be solved by the following equations with given C_{total}/C_i, G_{total}/G_i, R_c, and R_g.

$$\frac{C_{total}}{C_i} = \frac{R_c(1+(R_c-1)X')}{R_c-(R_c-1)Y'+(R_c-1)X'Y'}, \quad (14)$$

$$\frac{G_{total}}{G_i} = \frac{R_g(1+(R_g-1)X')}{R_g-(R_g-1)Y'+(R_g-1)X'Y'}. \quad (15)$$

The ratios of both C_{total}/C_i and G_{total}/G_i are given by the data of C/C_i and G/G_i. The ratios of both C_w/C_i and G_w/G_i are constants and can be determined experimentally. Here, R_c and R_g were set as 37 and 400, respectively. They were measured at 0 °C for water and –10 °C for ice, respectively.

Systems of equations (11)-(12) and (14)-(15) are quadratic for X' and Y' and, thus, return pairs of solutions. To choose a right pair we applied additional criteria: $0 \le X' \le 1$ and $0 \le Y' \le 1$, and a requirement of minimum LWCi.

Figures 9a&b show examples of the time-variations of LWCi as calculated with assumptions of the above four models. The results show that LWCi could vary depending on the connection model chosen. The combination models #1 and #2 have the similar results of LWCi. The reason is that the obtained X' and Y' showed the conditions of either $X' \ll Y'$ or $X' \gg Y'$ so that a term of $X'Y'$ become smaller than terms of X' and Y'. As the results, the difference between two combination models diminished.

The results also show that LWCi as calculated for the series model with use of the conductance data is unrealistically large and is not consistent with LWCi as calculated for the same series model with use of the capacitance data. Thus, we conclude that the series connection model is not suitable.

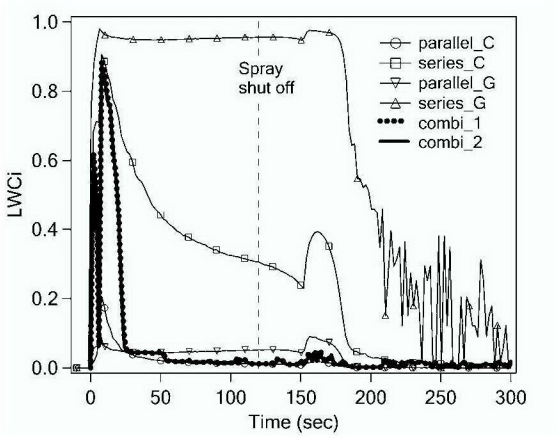

(a)

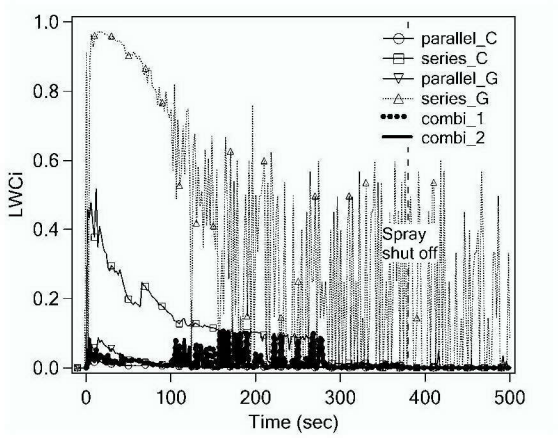

(b)

Figure 9. Time-variations of LWCi as calculated in four models. (a) Temperature = –10 °C, air speed = 115 km/h, water content in air = 1.67 g/m^3, and ice growth rate = 13.25x10^{-3} mm/sec. (b) Temperature = –30 °C, air speed = 115 km/h, water content in air = 0.25 g/m^3, and ice growth rate = 6.39x10^{-3} mm/sec.

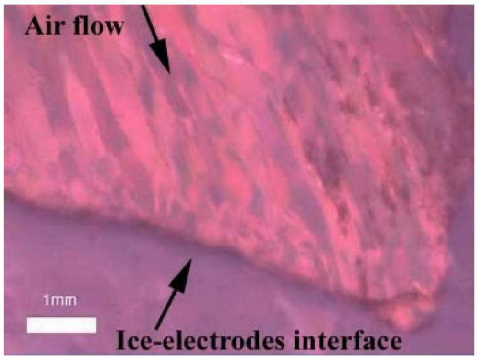

Figure 10. Thin section of atmospheric ice at high water rate conditions (75 km/h and 0.75g/m^3) and –10°C. Air flow was parallel to elongating column grains.

We found a similar inconsistency of LWCi calculated from *C*- and *G*-data for the parallel-connection model, see Fig. 9. But either of two combination-connection models returned consistent and reasonable values of LWCi. For that reason, we give that model our preference. Moreover, examination of ice microstructure using thin sections cut of grown ice samples also support the assumption of mixed mode in which unfrozen water channels (grain boundaries) oriented in the electrode vicinity, see Fig. 10. Figure 10 shows an example of thin sections of atmospheric ice at the high water rate (75km/h and 0.75g/m3) and –10 °C obtained by our previous test. Small grains were formed at the bottom of the ice sample and large columnar grains were formed on the small grains. There are also isolated round grains between columnar grains. This picture indicated that we dealt with some sort of combination of series and parallel connections of liquid and solid regions in the ice samples. Therefore, we may conclude that a combination of series and parallel connections of liquid and solid regions is most appropriate MODEL.

4. CONCLUSION AND FUTURE STUDY

In order to measure liquid water content in growing atmospheric ice (LWCi) in-situ, we relied on the known differences in electrical properties between water and ice and recorded the time-variation of the capacitance and conductance of atmospheric ice under a wide range of experimental conditions. We developed a data analysis method of LWCi for the time-variation of the samples' *C* and *G*, and then normalized the raw data for the sample thickness effect. LWCi could then be determined from the time-variation data for these electrical properties using a combination series and parallel connection model.

In our analysis method, we ignored the dependence on temperature of the dielectric constant and conductivity (i.e., R_c and R_g). However, the time-variations of *C* and *G* also reflect the sample's temperature changes during icing. Therefore, future study will involve taking this temperature dependence into account in order to further refine the data analysis method of LWCi. We will also perform similar experiments on grids of electrodes of various dimensions to investigate how LWCi varies with the distance from the interface.

ACKNOWLEDGMENTS

This research was supported by grant DAAD19-03-1-0078 from U.S.Army Research Office.

REFERENCES

Bragg, M.B., S. Lee, and C.M. Henze (1997) Heat transfer and freestream turbulence measurements for improvement of the ice accretion model. *AIAA Paper* No.1997-0053. Jan. 6–10, 1997, Reno, NV.

Druez, J., D.D. Nguyen, and Y. Lavoie (1987) Mechanical Properties of Atmospheric Ice, *Cold Region Science and Technology*, 13, 67–74.

Lozowski E.P. (2001) Physics and Mechanisms of Atmospheric Icing, Abstracts of an International Workshop on Physics and Mechanics of Ice II, 5&6 Marach 2001, Dartmouth College, Hanover, NH.

Minsk, L.D. (Ed.) (1983) Proc. First International Workshop on Atmospheric Icing of Structures. *CRREL Special Rep.*83–17.

Petrenko, V.F. and Whitworth, R.W. (1999) *Physics of Ice*, Oxford Univ. Press.